



Vibration Control of Corrugated Steel Web Box Girder Bridge with Friction Pendulum Isolation

Zhen Wang¹, Juntao Hu², Wei Jing^{2*} , Wendong Zhang¹

¹ China Construction Fourth Engineering Division Corp. LTD Guangzhou, Guangdong 510665, China.

² Western Engineering Research Center of Disaster Mitigation in Civil Engineering of Ministry of Education, Lanzhou University of Technology, Lanzhou 730050, China.

Received 30 June 2024; Revised 09 September 2024; Accepted 15 September 2024; Published 01 October 2024

Abstract

In order to investigate the feasibility and applicability of friction pendulum bearings for vibration control of large-span space beam-arch bridges with corrugated steel web box girders, taking the Huian Yellow River Bridge in Guide County, Qinghai Province, China, as an example. A three-dimensional calculation model of the friction pendulum isolation space beam-arch composite bridge with a corrugated steel web was established by MIDAS, the modal analysis was carried out, and the damping effect of the friction pendulum isolation bridge was investigated using the response spectrum and the time history analysis methods; the influence of the design parameters of the friction pendulum isolation on the reduction effect was further analyzed. The results show that the friction pendulum isolation improves the stress conditions of both the girder and the pier and reduces the displacement and acceleration of the pier top, as well as reduces the acceleration of the girder, and the damping ratio is more than 50%. The optimal dynamic coefficient of friction and the radius of curvature for the corrugated steel web composite bridge are 0.04 and 3.0 m, respectively. Friction pendulum isolation has a good seismic absorption effect and provides an effective way for the seismic control of the corrugated steel web composite bridge.

Keywords: Corrugated Steel Web Box Girder Bridge; Friction Pendulum Isolation; Response Spectrum; Time History Analysis.

1. Introduction

Recent earthquakes have been occurring frequently, especially in regions of high seismic risk, so bridge structures are at serious risk of damage. With the emergence of the corrugated steel web prestressed concrete composite box girder bridge, the seismic performance of the bridge structure reached a new height, and the structure has a unique position in the steel-prestressed concrete composite structure. The corrugated steel web box girder bridge has many advantages, such as light weight, saving materials, and beautiful appearance. At the same time, it also has a certain effect on improving the seismic capacity of the bridge structure. Therefore, this kind of bridge has a wide application prospect in earthquake-prone areas.

Bridge structure is prone to different degrees of damage under an earthquake. As a lifeline project, it is very necessary to ensure its safety under an earthquake. Because of its unique advantages, friction pendulum isolation has a good application prospect in bridge shock absorption. Zhan et al. [1] used ANSYS to establish a full-bridge model, investigated the effect of friction coefficient and curvature radius on the seismic responses of continuous beam bridges by the nonlinear time history analysis, and suggested that the resistance of the shear studs should preferably not be set

* Corresponding author: jingwei3276@163.com

 <http://dx.doi.org/10.28991/CEJ-2024-010-10-01>



© 2024 by the authors. Licensee C.E.J, Tehran, Iran. This article is an open access article distributed under the terms and conditions of the Creative Commons Attribution (CC-BY) license (<http://creativecommons.org/licenses/by/4.0/>).

too large. Zhang et al. [2] studied the dynamic characteristics and seismic effects of bridges under different seismic isolation schemes based on Midas and concluded that when the isolation scheme was applied to all piers, the best isolation performance of friction pendulum bearing was achieved. He et al. [3] established and studied the prototype bridge of the typical simply supported girder bridges in China, compared the seismic responses of friction pendulum bearing (FPB) isolated and non-isolated bridges, and presented a new criterion index to quantifiably measure the effectiveness of the seismic isolation of FPB isolated bridges with different pier heights. Li et al. [4] investigated the influence of the friction coefficient and isolation period of the FPB on the response of isolated bridges under multi-hazard source excitations and concluded that the energy dissipation capacity of FPB in isolated bridges was excellent. Chen et al. [5] investigated the feasibility and efficiency of base isolation by implementing FPBs at the bottom of tall piers and recommended a larger value of radius of concave surface for designing. Meng et al. [6] investigated the effect of transverse pounding on a bridge isolated by FPBs using 1:6 large-scale shake table tests and concluded the lateral pounding should be considered in the design of isolated bridges.

Gino et al. [7] investigated the seismic reliability of multi-span continuous deck bridges equipped with FPBs. Gupta et al. [8] evaluated a continuously curved bridge equipped with FPS under various earthquake loadings, performed a sensitivity analysis, and concluded that FPBs significantly reduced the bridge seismic responses. Zhao et al. [9] proposed a new type of rotating mass friction damper (RMFD) with an amplification effect and a negative stiffness effect and used SAP2000 software to compare and analyze the seismic responses, damping rate, and displacement control effect under large earthquakes. Li et al. [10] analyzed the seismic responses of the 6×110 m long-span continuous girder bridge under different wear degrees of FPB. Wang et al. [11] conducted an experimental study on the shear force of the shear pin device in practical bridge engineering applications and analyzed the law of the influence of the friction force on the shear force of the shear pin when the horizontal bearing capacity of the FPB reached the initial force required for its vibration reduction and isolation function. Cao et al. [12] used an adaptive stiffness isolator on a typical multi-span bridge structure, analyzed its response under bi-directional ground motion records, and concluded that the isolators significantly reduced base shear forces. Wei et al. [13] designed two kinds of variable curvature friction pendulum bearings (VFPB) with adaptive ability and concluded that the maximum residual displacement of the bearing was related to the friction coefficient and the first derivative of the shape function of the sliding surface. Chang et al. [14] proposed a tunable friction pendulum system (TFPS) to study its seismic isolation control performance in bridge structure.

Some researchers have also carried out related research on the corrugated steel web bridge with friction pendulum bearings. Liu et al. [15], based on the Hanjiang Bridge of the Xiangyang Ring Expressway, adopted the composite seismic measures of speed locker + FPB and optimized the design of the relevant parameters of the bearing based on Midas. Han et al. [16] conducted a seismic fragility assessment of prestressed concrete composite girder bridges with corrugated steel webs under near-fault pulse-like ground motions and concluded that the bridges with corrugated steel webs are less vulnerable than the concrete bridges, and the shock absorption effect of the friction pendulum bearing was better than that of the viscous damper.

To sum up, there are many studies on the friction pendulum isolation bridges, but there are few studies on the large-span space beam-arch corrugated steel web box girder bridges using friction pendulum isolation, so it is necessary to further study the damping performance and the corresponding influencing factors of the corrugated steel web bridge with friction pendulum bearing. In this paper, taking the Huian Yellow River Bridge in Guide County, Qinghai Province, China, as the research object, a 3-D calculation model of the corrugated steel web composite bridge was established by using MIDAS, and the modal analysis was carried out firstly, and then the dynamic characteristics and response of the bridge under the conditions of ordinary fixed bearing and friction pendulum isolation were studied by using the response spectrum method and the time history analysis method, respectively. The influence of the design parameters of the friction pendulum isolation on the seismic isolation performance of the bridge was analyzed, and some suggestions for the design of optimal parameters were also given. By analyzing the dynamic responses of corrugated steel web box girder bridges, it is helpful to better understand the mechanical behavior under earthquakes, which can provide useful experience and guidance for the design and damping control of similar bridges. The flowchart of the methodology process is shown in Figure 1.

2. Project Overview

The Huian Yellow River Bridge is located in Guide County, Qinghai Province, China. The bridge is a key project and livelihood project, as shown in Figure 2. The length of the main bridge is (60+3×103+60) m, and the prestressed concrete structure of corrugated steel web is used. The completion of the bridge will be of great significance to the development of the transportation industry in Guide County. The bridge girder is a five-span, variable-height, continuous beam using prestressed concrete and a corrugated steel web. The seismic fortification intensity of the bridge is 7 degrees, the seismic acceleration is 0.15 g, the site characteristic period is 0.40 s, and the maximum horizontal seismic influence coefficient is 0.12.

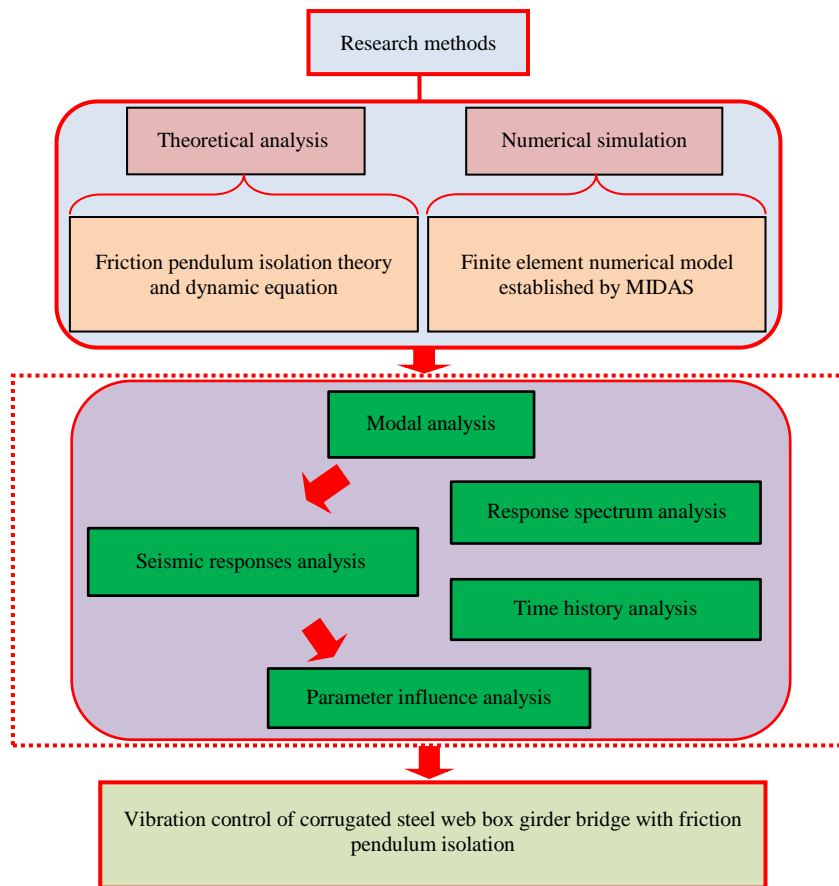


Figure 1. Flowchart of methodology process

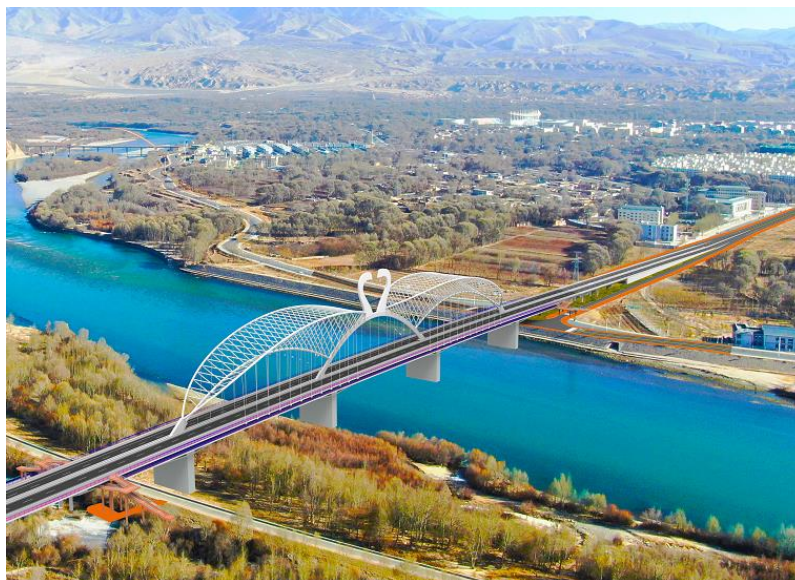


Figure 2. Huian Yellow River Bridge in Guide County

3. Friction Pendulum Isolation

The simplified calculation model of the friction pendulum bearing is shown in Figure 3. Under the action of an earthquake, when the component force of the hinged slide block in the tangential direction is greater than the bounding static friction force on its bottom, the slider will move back and forth on the sliding surface. Equation 1 can be used to represent the equation of moment equilibrium of the slider at the center of the circle [17]:

$$FR\cos\theta = WD + fR \tag{1}$$

where F is the horizontal restoring force; f is the sliding friction; R is the sliding radius; D is the maximum amount of slippage; W is the vertical load borne by the bearing; θ is the vertical included angle.

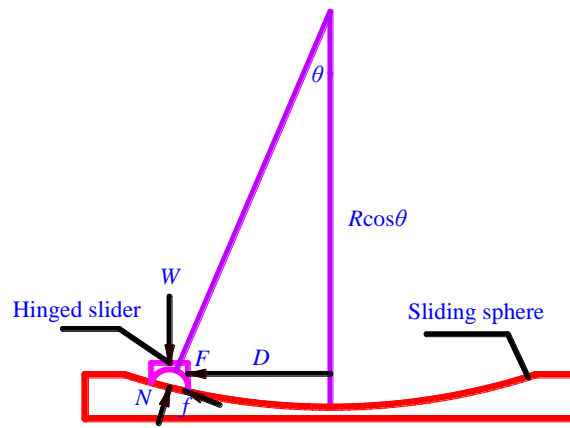


Figure 3. Simplified model of friction pendulum bearing

Since the friction pendulum isolation is very small in actual operation, F can be simplified to Equation 2:

$$F = \frac{WD}{R} + \mu_d W \tag{2}$$

where μ_d is the coefficient of dynamic friction.

Finally, the equivalent shear stiffness of the friction pendulum bearing can be calculated according to Equation 3:

$$k_{eff} = \frac{W}{R} + \frac{\mu_d W}{D} \tag{3}$$

where k_{eff} is the equivalent shear stiffness of the friction pendulum isolation

After repeating calculations and verifications, the main design parameters of the friction pendulum bearing are as follows: the sliding radius of the friction pendulum isolation is set to 2 m; the coefficient of friction is 0.03 when moving at low speed; in the case of fast movement, the coefficient of friction is 0.05; the maximum slippage is 300 mm.

4. Numerical Calculation Model

The arch rib span of the middle span is 103 m, the vector height is 24.5 m, the vector span ratio is 1/4.2, and the arch axis is a quadratic parabola. The edge span arch rib span is 112.5 m, the vector height is 24 m, the vector span ratio is 1/4.7, and the arch axis is a quadratic parabola. The subarch of the side span is a space arch, the projection span of the facade is 147 m, the vector height is 38, the arch axis is an arc line with a radius of 120 m, and the plane projection is a numerically fitted hexid parabola. The suspension cables are extruded with steel strands in whole, with 32 strands of vertical suspension cables and 48 strands of diagonal suspension cables. The specifications of the suspension cables are 1860 MPa epoxy steel strands with a diameter of 15.2 mm. The thickness of the corrugated steel web is 12-26 mm. A three-dimensional numerical calculation model of the large-span space beam-arch composite bridge with a corrugated steel web was established by MIDAS/Civil, as shown in Figure 4. Considering that the bridge is mainly shear during the stress process, the steel web is equivalent to a concrete web with a thickness of 10 mm according to the equivalent interface law [18]. The main girder of the bridge has a total of 162 structure elements and 199 nodes. The whole bridge is supported by friction pendulum bearings, and the friction pendulum bearings are arranged at the positions of abutments and piers, and a total of 18 friction pendulum bearings are arranged. Parameters of the friction pendulum bearing are shown in Table 1. In order to study the damping effect of the bridge structure, a comparison model is established by using the conventional fixed bearing, and the main girder is rigidly connected with the bridge pier in the numerical simulation model.

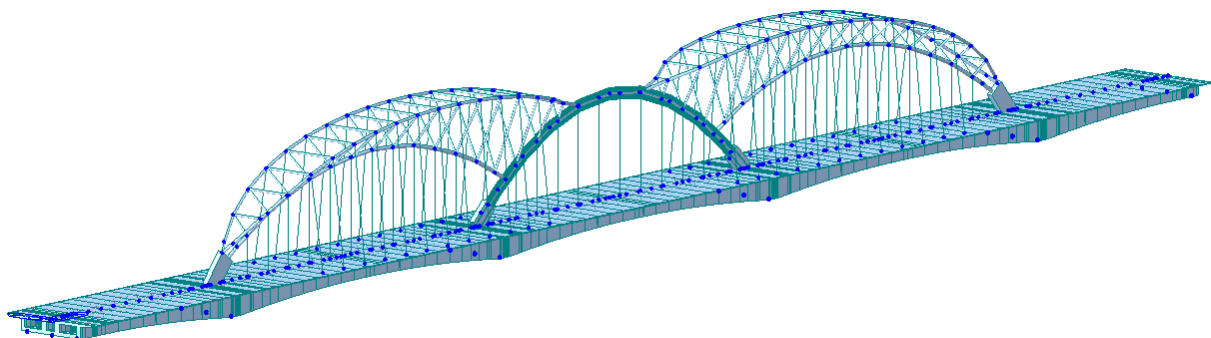


Figure 4. Numerical calculation model

Table 1. Friction pendulum bearing parameters

Type	1	2
Pier number	6, 7, 8, 9	5, 10
Coefficient of static friction	0.03	0.02
Coefficient of dynamic friction	0.05	0.03
Radius of curvature (m)	2.0	1.8

5. Modal Analysis

The finite element equation is obtained by superimposing the inertial force, damping force and elastic force of each element:

$$[M]\{\ddot{\delta}\} + [C]\{\dot{\delta}\} + [K]\{\delta\} = [P] \tag{4}$$

where $[M]$ is the mass matrix; $[C]$ is the damping matrix; $[K]$ is the stiffness matrix; $[P]$ is the load array.

When the free vibration $[P] = 0$ and the damping force is ignored, then Equation 4 becomes the free vibration Equation of the system:

$$[M]\{\ddot{\delta}\} + [K]\{\delta\} = [P] \tag{5}$$

In the case of free vibration, taking the displacement $\{\delta\}=[A]\cos\omega t$ into Equation 5:

$$([K] - \omega^2[M])[A] = \{0\} \tag{6}$$

where A is the amplitude; ω is the natural frequency.

The amplitude $[A]$ cannot all be zero in the case of free vibration, so a value of 0 for the coefficient matrix determinant in Equation 6:

$$|[K] - \omega^2[M]| = 0 \tag{7}$$

In the case of a large number of degrees of freedom in finite element analysis, it is difficult to solve the n -th order Equation 7, so it can be solved by the method of mathematical eigenvalue [19]. In this study, the eigenvalue analysis of the corrugated steel web box girder bridge is carried out by using the subspace iterative method.

For the purpose of studying the seismic isolation effect of the friction pendulum isolation, the friction pendulum bearing is replaced by an ordinary fixed bearing, in which the girder is rigidly connected with the bridge pier. The dynamic characteristics of corrugated steel web box girder bridges under two different bearings are compared. Table 2 shows the vibration frequencies of the first ten-orders of the modal under the two bearings.

Table 2. Comparison of vibration frequencies of the first ten-orders

Modal order	Friction pendulum bearing	Ordinary fixed bearing	Difference ratio
1	1.037	1.256	22.3%
2	1.543	1.989	29.1%
3	2.182	2.389	9.8%
4	2.421	2.858	18.5%
5	2.953	3.986	35.0%
6	3.707	4.109	10.9%
7	4.111	4.442	8.1%
8	4.441	5.019	13.1%
9	5.020	6.150	22.4%
10	6.716	7.780	16.1%

From Table 2, it can be seen that with the increase of modal order, the vibration frequencies corresponding to the friction pendulum bearing and ordinary fixed bearing are significantly different. In general, from the first-order mode to the tenth-order mode, the vibration frequency of the structure with the friction pendulum isolation is always lower than that of the latter, and the relative difference can reach up to 35.0%. The results show that the friction pendulum isolation has a significant effect in prolonging the vibration period of the structure. Moreover, it can reduce the structural natural vibration frequency, which is very important to reduce the seismic response of the bridge.

6. Seismic Responses Analysis

6.1. Response Spectrum Method

6.1.1. Basic Theory

In a single-degree-of-freedom system, the displacement δ_g of the ground results in a single point of mass vibration, and according to D'Alembert's principle, the motion equation is expressed as [20]:

$$m(\ddot{\delta}_g + \ddot{y}) + c\dot{y} + ky = 0 \tag{8}$$

where m is the mass; \ddot{y} is the acceleration; c is the damping; \dot{y} is the velocity; k is the stiffness; y is the displacement.

In the Equation 8, the inertial force, damping ratio, and elastic recovery force should be balanced. It can be obtained after transformation:

$$\ddot{y}(t) + 2\xi\omega\dot{y}(t) + \omega^2y(t) = -\ddot{\delta}_g \tag{9}$$

where $\xi = c/(2\sqrt{k \cdot m})$; $\omega = \sqrt{k/m}$.

For the seismic relative displacement response of a single-degree-of-freedom system, the Duhamel's integral is:

$$y(t) = -\frac{1}{\omega_d} \int e^{-\xi\omega(t-\tau)} \ddot{\delta}_g(\tau) \sin \omega_d (t - \tau) d\tau \tag{10}$$

where $\omega_d = \sqrt{1 - \xi^2}\omega_0$.

The integral expressions for relative velocity and acceleration under seismic action are obtained by Equations 11 and 12:

$$\dot{y}(t) = \int e^{-\xi\omega(t-\tau)} \ddot{\delta}_g(\tau) \left[\frac{\xi\omega}{\omega_d} \sin \omega_d (t - \tau) - \cos \omega_d (t - \tau) \right] d\tau \tag{11}$$

$$\ddot{y}(t) = \omega_d \int e^{-\xi\omega(t-\tau)} \ddot{\delta}_g(\tau) \left\{ \left[1 - \left(\frac{\xi\omega}{\omega_d} \right)^2 \right] \sin \omega_d (t - \tau) + 2 \frac{\xi\omega}{\omega_d} \cos \omega_d (t - \tau) \right\} d\tau - \ddot{\delta}_g(t) \tag{12}$$

In general, the Equations 11 and 12 can be simplified as:

$$\dot{y}(t) = - \int e^{-\xi\omega(t-\tau)} \ddot{\delta}_g(\tau) \cos \omega_d (t - \tau) d\tau \tag{13}$$

$$\ddot{y}(t) = \omega_d \int e^{-\xi\omega(t-\tau)} \ddot{\delta}_g(\tau) \sin \omega_d (t - \tau) d\tau - \ddot{\delta}_g(t) \tag{14}$$

6.1.2. Response Spectrum

According to the seismic design concept of two-level fortification and two-stage design in the Guidelines for Seismic Design of Highway Bridges (JTG/T B02-01-2008) [21], the seismic action is divided into two levels: E1 and E2. Among them, the E1 is a short-lived earthquake, and the E2 is with a long return period. In this paper, the response of the Huian Yellow River Bridge in Guide County under the action of the E2 earthquake is analyzed, the S_{max} is calculated to be 6.251 m/s², and Figure 5 shows the acceleration response spectrum curve. Calculation of the dynamic responses of bridge structure under E2 earthquake with the above-mentioned parameters, the input in the forward direction of the bridge is considered. These calculation results and analyses will help to evaluate the seismic performance of bridge structures under seismic action and provide important references for bridge design and improvement.

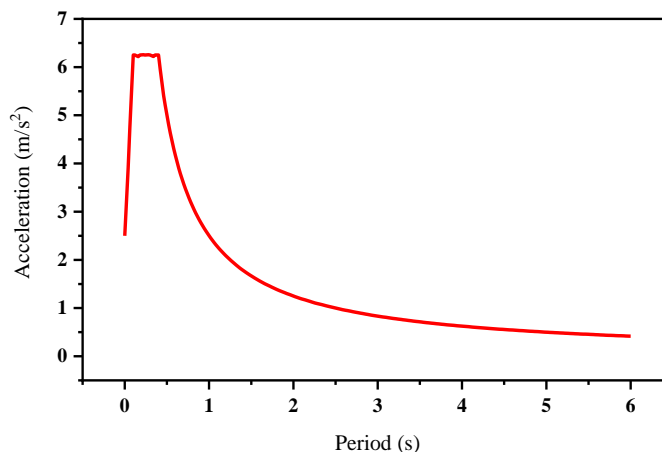


Figure 5. Horizontal acceleration response spectrum

6.1.3. Seismic Responses along Bridge

The displacement curves of the main beam under the action of the longitudinal bridge earthquake are shown in Figure 6. It can be obtained that the maximum transverse, vertical, and longitudinal displacements occur at the mid-span position. Regardless of whether friction pendulum bearings or conventional fixed bearings are employed, under the E2 earthquake scenario, the longitudinal displacement of the bridge structure exhibits the greatest magnitude, followed by the lateral and the vertical displacements. Furthermore, the peak displacement values of the corrugated steel web box girder bridge for both types of supports demonstrate a symmetrical distribution pattern along the mid-span, attaining their maximum at this location and subsequently decreasing towards the side spans. When using the ordinary fixed bearing, because of the large stiffness of the bearing, the substructure plays a stronger restraining effect on the superstructure, so that the peak value of the displacement response of the main beam under the ordinary fixed bearing is much smaller than that of the friction pendulum isolation.

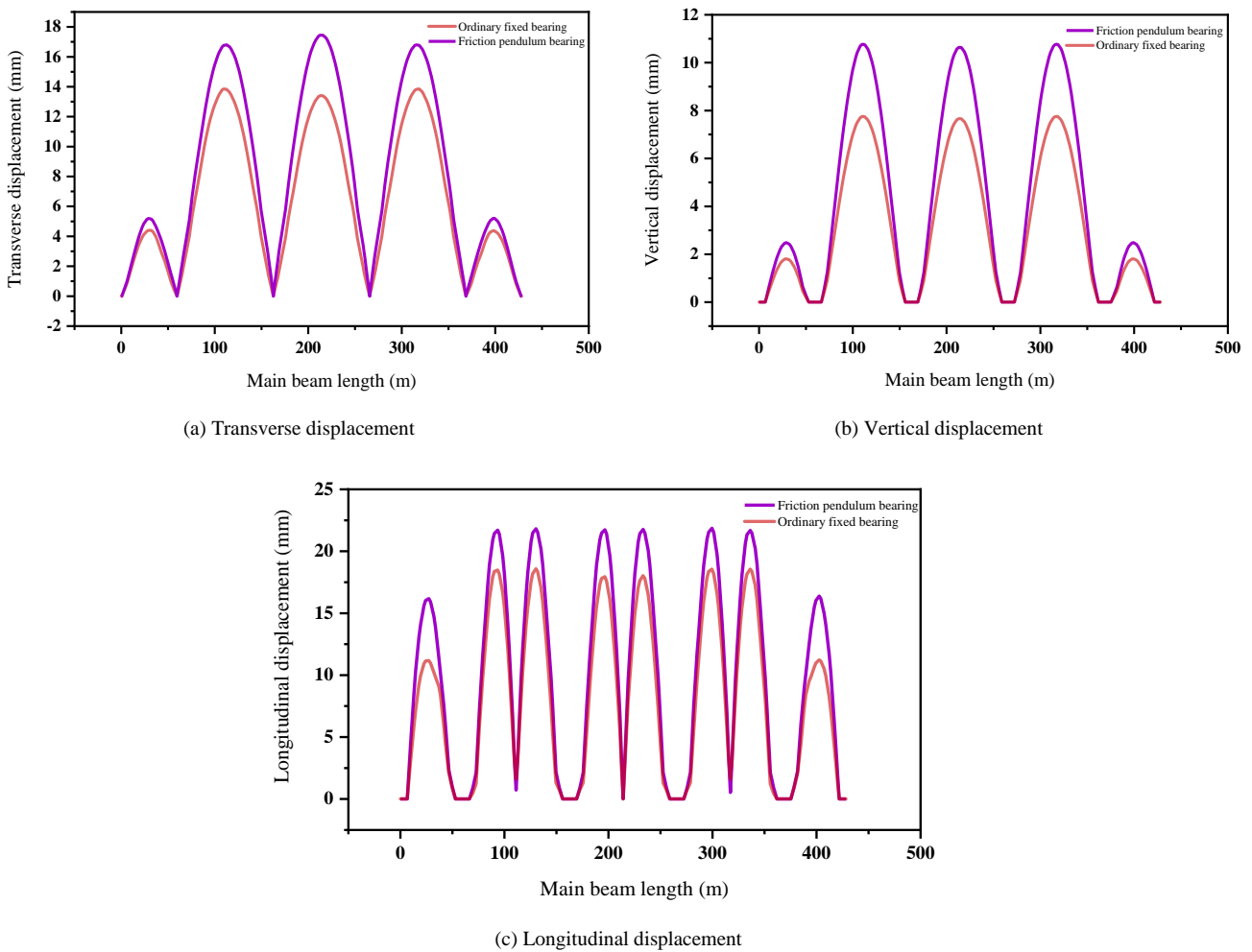


Figure 6. Displacement of main beam under E2 earthquake along the bridge

When the ground motion E2 is input along the bridge, the bending moment envelope diagram of the main beam of the corrugated steel web box girder bridge is shown in Figure 7. Regardless of the ordinary fixed bearings or the friction pendulum bearings are used, the largest bending moment takes place at the supporting position of the four middle piers, and the adjacent beam segments bear most of the bending moment, while the side spans and middle spans bear relatively small bending moment. On the whole, the bending moment of the main beam with friction pendulum bearings is smaller than that of ordinary fixed bearings in most cases. Therefore, by using the friction pendulum isolation, it is possible to reduce the bending moment in the cross section of the bearing. Moreover, it has a slight adjustment effect on the bending moment distribution of the side span and the middle span, so as to make the force of the whole bridge be more reasonable and the seismic performance be better.

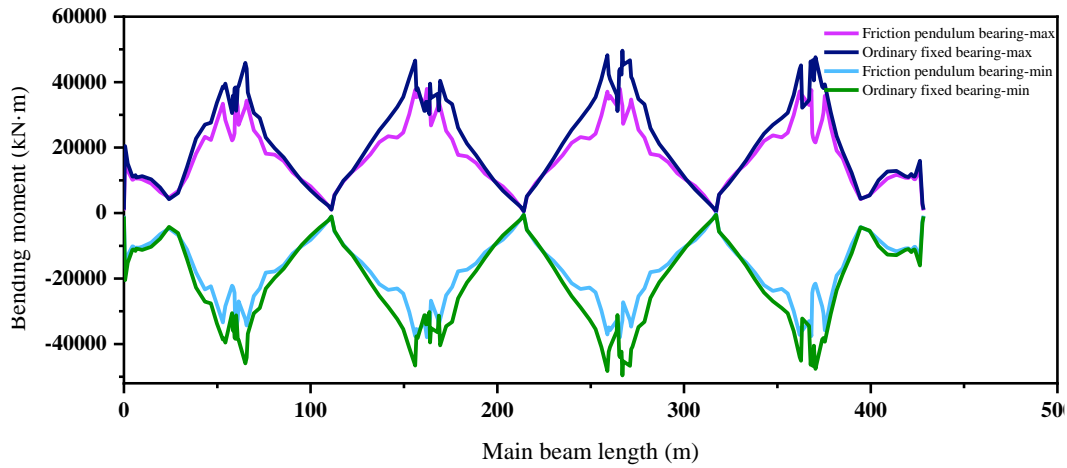


Figure 7. Envelope diagram of main beam bending moment under E2 earthquake along bridge direction

6.2. Time History Analysis

6.2.1. Dynamic Equation and Solution

The dynamic equation of bridge under earthquake action is shown in Equation 15:

$$M\ddot{U} + C\dot{U} + KU = F_e \tag{15}$$

Newmark- β method [22] is used for the solution of Equation 15, the method is a step-by-step integration method developed on the basis of linear acceleration method, and which can be applied to solve all kinds of nonlinear problems. Firstly, it is assumed that:

$$\dot{U}_{i+1} = \dot{U}_i + [(1 - \beta)\ddot{U}_i + \beta\ddot{U}_{i+1}]\Delta t \tag{16}$$

$$U_{i+1} = U_i + \dot{U}_i\Delta t + \left[\left(\frac{1}{2} - \gamma\right)\ddot{U}_i + \gamma\ddot{U}_{i+1}\right]\Delta t^2 \tag{17}$$

where β and γ are the adjustment coefficients introduced for consideration of accuracy and stability. When $\beta=0.5$ and $\gamma=0.25$, it is equivalent to the constant average acceleration method, that is, when the time is increased from t to $t+\Delta t$, the speed remains constant, namely, $(\dot{U}_i + \dot{U}_{i+1})/2$. Existed research have shown that when $\beta \geq 0.5$ and $\gamma \geq 0.25(0.5 + \beta)$, Newmark- β method is unconditionally stable.

The increment form $\Delta\dot{U}$ and ΔU of velocity \dot{U} and displacement U can be obtained by Equation 16 and Equation 17:

$$\Delta\dot{U}_i = \dot{U}_{i+1} - \dot{U}_i = (\ddot{U}_i + \beta\Delta\ddot{U}_i)\Delta t \tag{18}$$

$$\Delta U_i = U_{i+1} - U_i = \dot{U}_i\Delta t + \frac{1}{2}\ddot{U}_i\Delta t^2 + \gamma\Delta\ddot{U}_i \tag{19}$$

Increment of acceleration $\Delta\ddot{U}_i$ can be obtained by transforming Equation 19, then taking $\Delta\ddot{U}_i$ into Equation 18:

$$\Delta\ddot{U}_i = \frac{1}{\gamma\Delta t^2}\Delta U_i - \frac{1}{\gamma\Delta t}\dot{U}_t - \left(\frac{1}{2\gamma} - 1\right)\ddot{U}_t \tag{20}$$

$$\Delta\dot{U}_i = \frac{\beta}{\gamma\Delta t}\Delta U_i + \left(1 - \frac{\beta}{\gamma}\right)\dot{U}_t + \left(1 - \frac{\beta}{2\gamma}\right)\Delta t\ddot{U}_t \tag{21}$$

The incremental form of dynamic Equation 15 can be expressed as:

$$M\Delta\ddot{U}_i + C\Delta\dot{U}_i + K\Delta U_i = \Delta F_{e(i)} \tag{22}$$

Taking Equations 19 to 21, then Equation 22 can be obtained:

$$\bar{K}\Delta U_i = \bar{F} \tag{23}$$

where $\bar{K} = K + \frac{1}{\gamma\Delta t^2}M + \frac{\beta}{\gamma\Delta t}C$; $\bar{F} = \Delta F_{e(i)} + M\left[\frac{1}{\gamma\Delta t}\dot{U}_i + \left(\frac{1}{2\gamma} - 1\right)\ddot{U}_i\right] + C\left[\left(\frac{\beta}{\gamma} - 1\right)\dot{U}_i + \left(\frac{\beta}{2\gamma} - 1\right)\Delta t\ddot{U}_i\right]$.

The increment of displacement ΔU_i can be obtained by Equation 23, and the increment of velocity $\Delta\dot{U}_i$ can be obtained by taking ΔU_i into Equation 21, then displacement and velocity of $i+1$ time step can be obtained:

$$U_{i+1} = U_i + \Delta U_i \quad (24)$$

$$\dot{U}_{i+1} = \dot{U}_i + \Delta \dot{U}_i \quad (25)$$

The acceleration \ddot{U}_{i+1} of $i+1$ time step can be obtained by taking Equation 24 and Equation 25 into Equation 15:

$$\ddot{U}_{i+1} = M^{-1} \cdot [F_e - C \cdot \dot{U}_{i+1} - K \cdot U_{i+1}] \quad (26)$$

6.2.2. Seismic Waves

Based on the time history analysis, the seismic responses of the corrugated steel web box girder bridge are analyzed. The earthquake duration is 60s, the interval is 0.02s, and the damping ratio is 0.05. In this paper, the El-Centro wave and the Taft wave are input in three directions to calculate the seismic responses. The earthquake acceleration time history curves are shown in Figures 8 and 9.

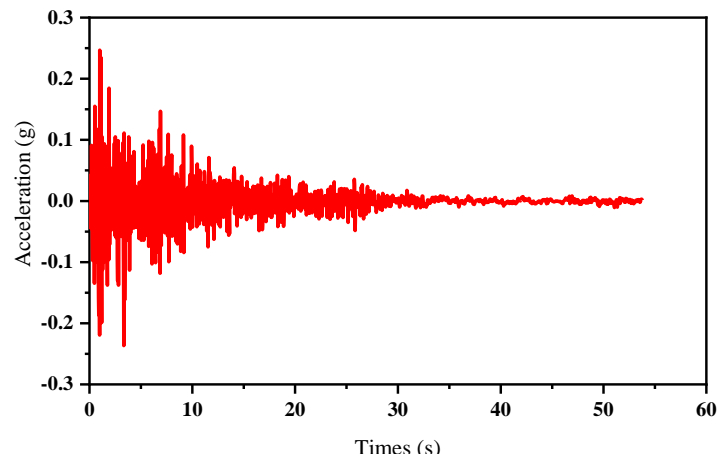


Figure 8. El-Centro wave

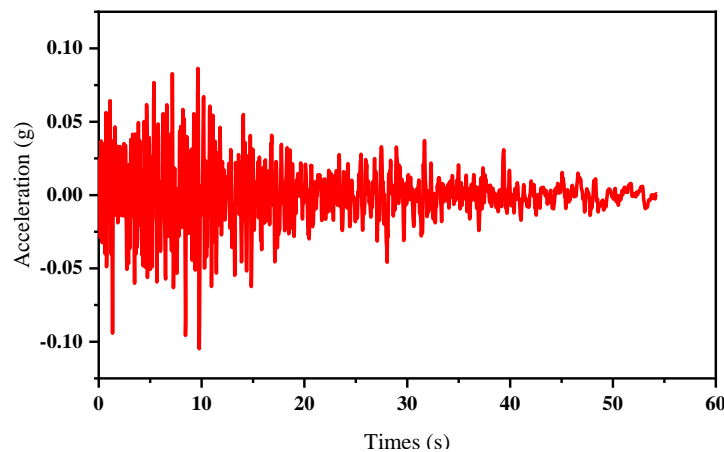


Figure 9. Taft wave

6.2.3. Displacement and Acceleration

Under the El-Centro wave and Taft wave, the displacement and acceleration time-history curves of the main beam and pier top of the corrugated steel web box girder bridge are shown in Figures 10 to 13. When the ordinary fixed bearings are adopted, the restraint ability of the substructure to the superstructure is significantly enhanced because the bearing itself has a large stiffness, so that a more reliable restraint mechanism is provided, and the peak value of the displacement response of the main beam is relatively small. Furthermore, compared with the main beam with the ordinary fixed support design, the bridge with friction pendulum isolation exhibits higher friction characteristics under seismic action, resulting in a relatively small peak acceleration response of the bridge pier. The results indicate that although both of them can provide steady support for the main beam under an earthquake, the design of the friction pendulum isolation is more inclined to guarantee the whole stability and security of the structure. This design concept is critical for bridge structures in earthquake-prone areas because it can reduce post-earthquake damage while maintaining structural integrity.

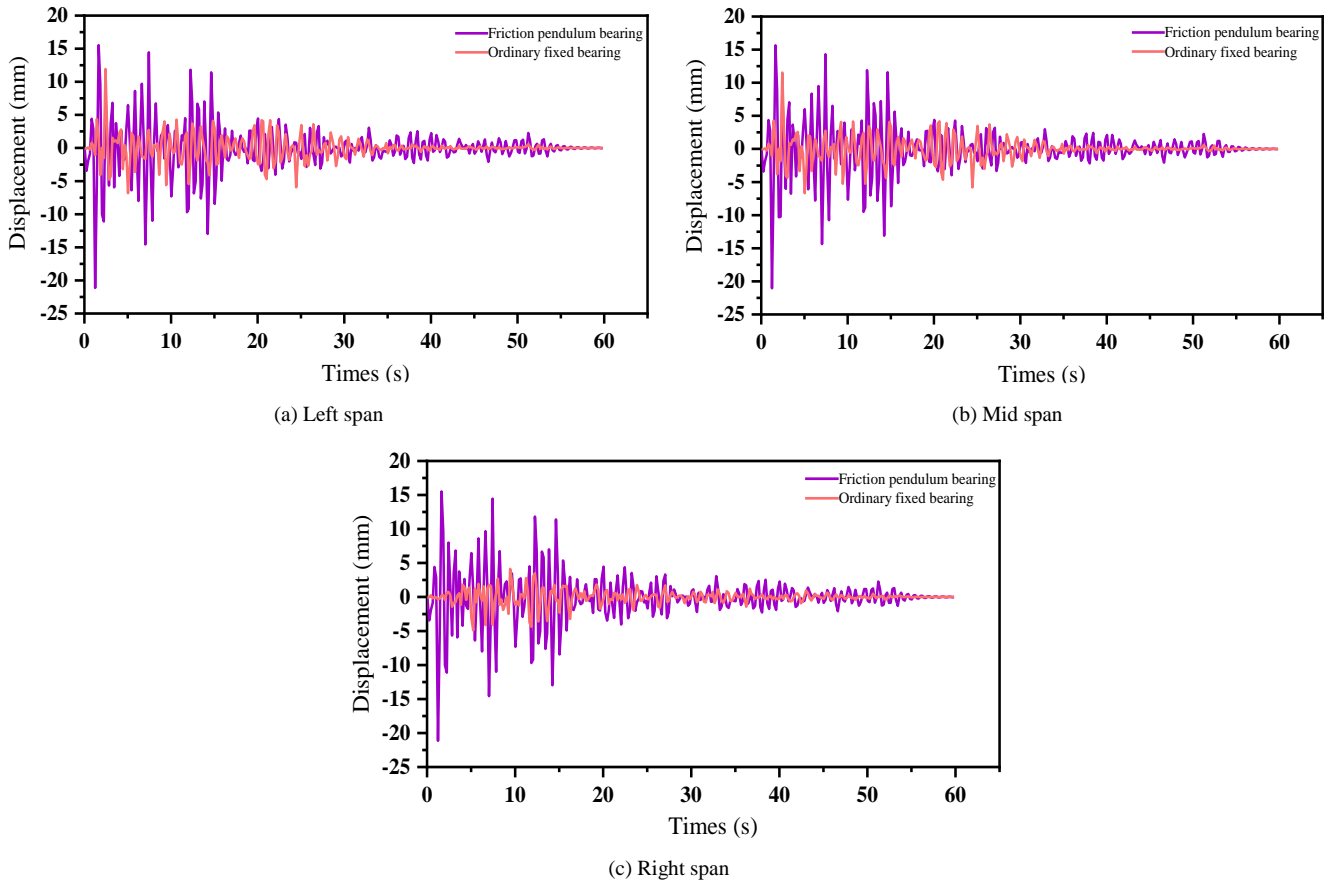


Figure 10. Time history of mid-span displacement under El-Centro wave

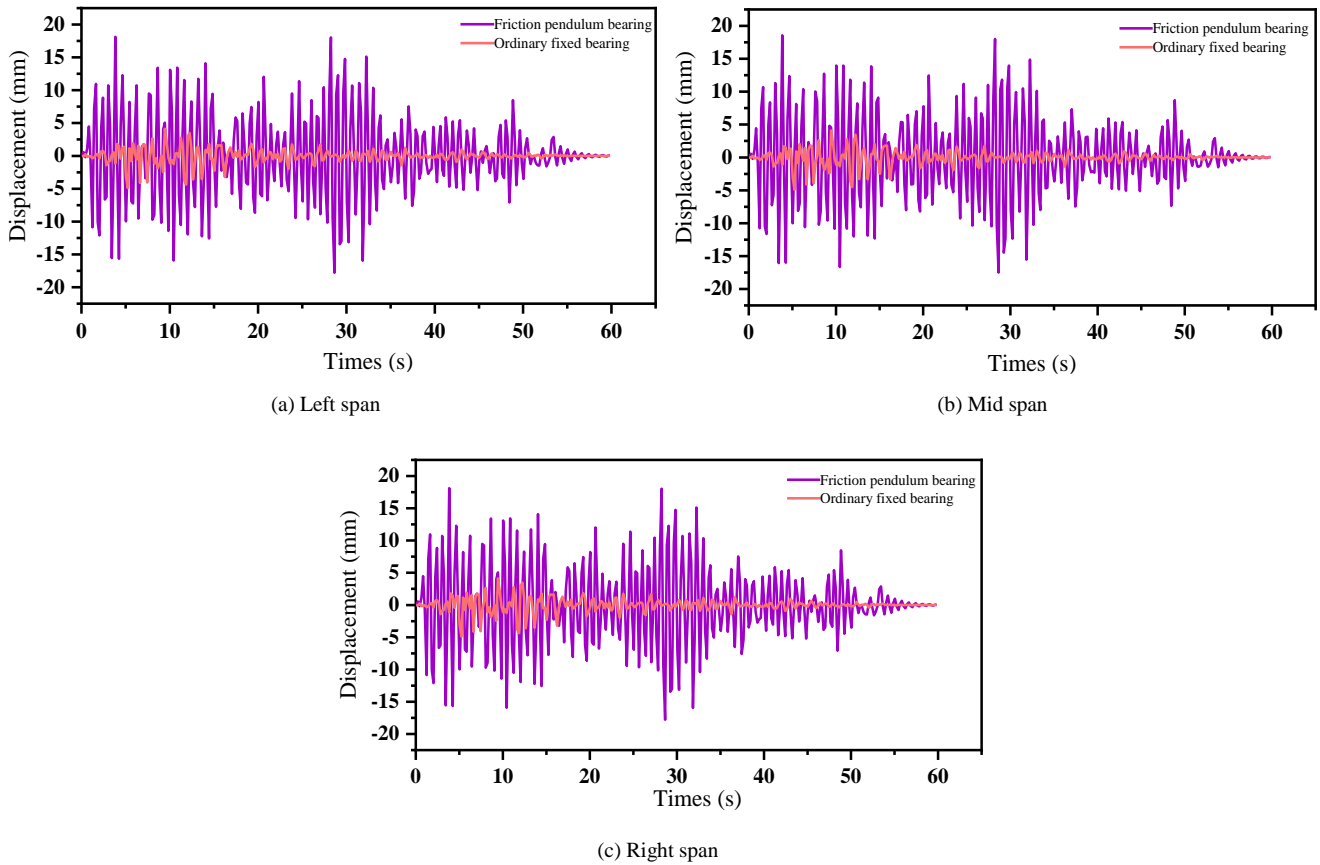


Figure 11. Time history of mid-span displacement under Taft wave

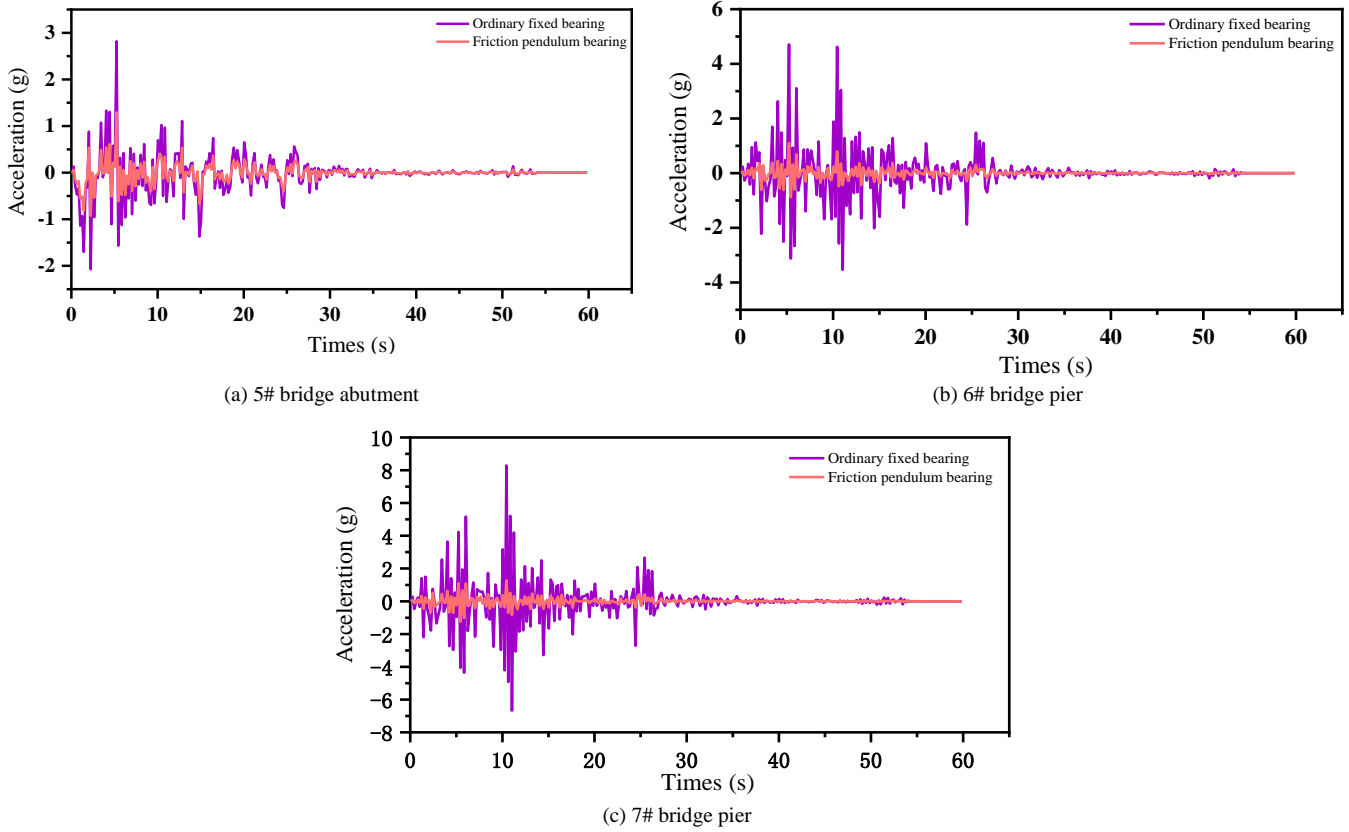


Figure 12. Pier acceleration time history under El-Centro wave

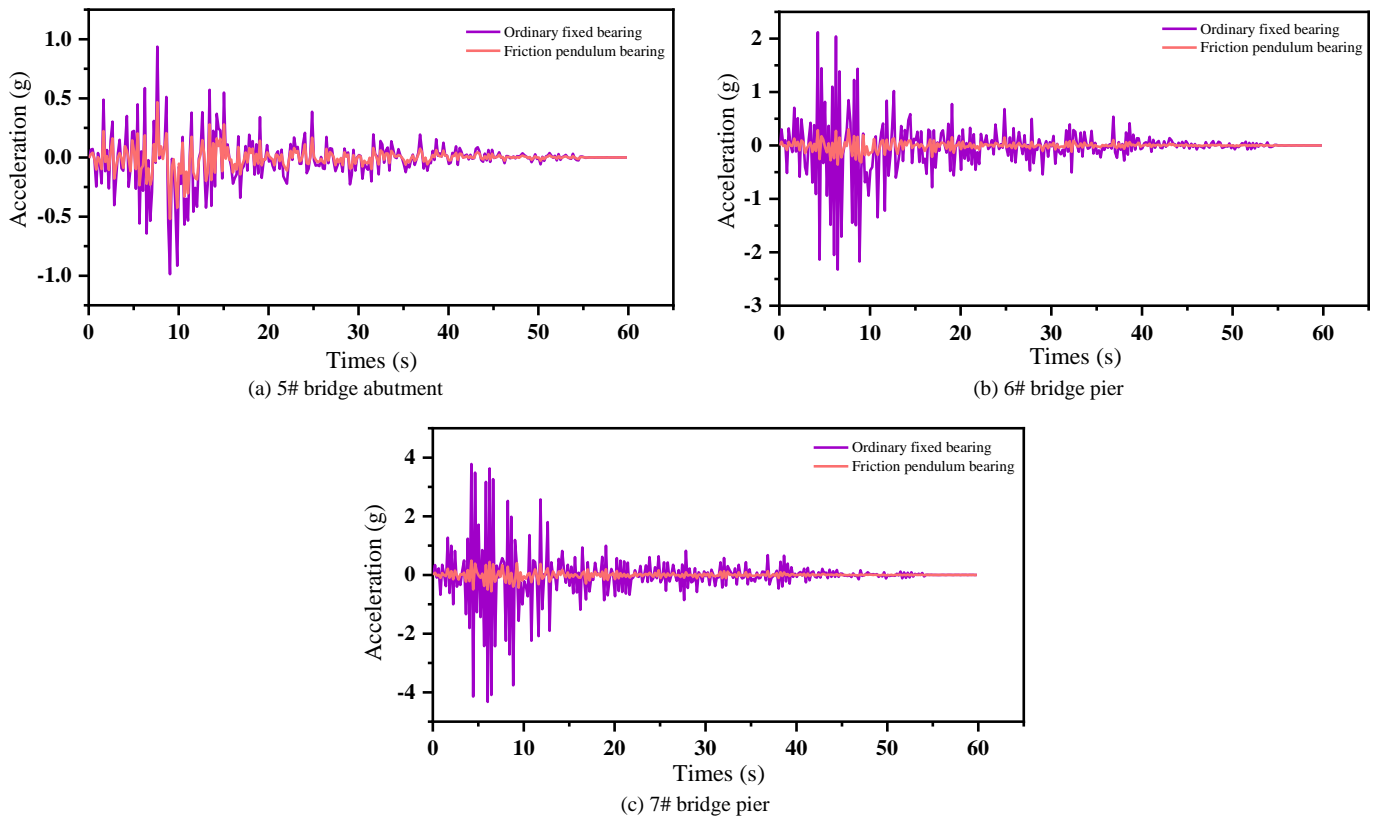


Figure 13. Pier acceleration time history under Taft wave

Due to the symmetry on both sides of the bridge, Table 3 only shows the displacement and acceleration of the pier peak of the three piers under the effect of the El-Centro wave and Taft wave. It can be seen that the displacement and acceleration of the pier crest corresponding to the bridge with friction pendulum bearings are significantly reduced, and the damping ratio is more than 50%. In conclusion, the friction pendulum isolation can significantly reduce the

displacement and acceleration of the pier top, which fully demonstrates the effectiveness and superiority of the friction pendulum isolation in shock absorption of this kind of bridge.

Table 3. Shock absorption effect of friction pendulum isolation

Location	Type	Displacement (mm)		Damping ratio		Acceleration (m/s ²)		Damping ratio	
		El-Centro	Taft	El-Centro	Taft	El-Centro	Taft	El-Centro	Taft
5# abutment top	Ordinary fixed bearing	30.9	25.6	60.2%	61.7%	2.886	1.056	54.5%	53.3%
	Friction pendulum isolation	12.3	9.8			1.312	0.493		
6# Pier top	Ordinary fixed bearing	42.5	36.5	52.2%	51.5%	4.430	2.222	71.1%	62.8%
	Friction pendulum isolation	20.3	17.7			1.279	0.826		
7# Pier top	Ordinary fixed bearing	54.9	46.8	58.5%	59.6%	4.392	3.906	69.8%	68.6%
	Friction pendulum isolation	22.8	18.9			1.326	1.226		

In general, while both types of supports can provide stable reinforcement for the main beam during seismic events, the design of friction pendulum bearings is more focused on ensuring the overall stability and safety of the structure rather than solely depending on the localized impact forces. This design philosophy is crucial for bridge structures subjected to seismic effects, as it mitigates post-earthquake damage while preserving structural integrity.

7. Parameter Influence Analysis

According to the mechanical properties of the friction pendulum bearing, the two key factors affecting the seismic reduction and isolation effect are the curvature radius R and the dynamic friction coefficient μ . The isolation period of the friction pendulum isolation is dependent on the R , and increasing the R can effectively extend the isolation period. Therefore, based on the finite element model of the Huian Yellow River Municipal Bridge in Guide County, the parameters analysis of the R of and the μ of the isolation bearing is carried out [23].

The design pressure of the sliding surface can be determined by Equation 27:

$$\sigma = \frac{F}{2\pi R h} \leq [\sigma] = 30 \text{MPa} \quad (27)$$

where R is the curvature radius; h is the ball crown height; F is the bearing pressure; σ is the design pressure.

The ball crown height h of the sliding surface can be approximated to take 1/4-1/5 of the bearing height, and the minimum radius of curvature of the friction pendulum bearing can be obtained by using the allowable stress method:

$$R \geq \frac{F}{2\pi[\sigma]h} = \frac{50000}{2 \times \pi \times 30 \times 10^3 \times 0.125} = 2.12 \text{ m} \quad (28)$$

In addition, the maximum curvature radius of the sliding surface can be determined by the maximum allowable displacement of the bearing. The design experience shows that for continuous beam bridges with span of 50m-150m, the post-flexion stiffness is roughly between 4000 kN/m-10000 kN/m, from which the maximum radius of curvature can be determined.

$$R \leq \frac{W}{K} = \frac{50000}{4000} = 12.5 \text{ m} \quad (29)$$

where W is the post-flexion stiffness.

Therefore, $2 \text{ m} \leq R \leq 12 \text{ m}$ is adopted. In this paper, the curvature radius R is set as 2 m, 3 m, 4 m, 6 m, 8 m and 10 m. Besides, the range of the dynamic friction coefficient for the bridge bearing is 0.01-0.12.

The previous results show that the internal force of the pier top and the displacement of the main beam are similar under the action of the El-Centro wave and the Taft wave, so only the response under El-Centro wave action is used as the analysis object in this section. The effects of the μ and R on the maximum displacement of the main beam, maximum displacement of the pier top, and bending moment of the 6# pier top are shown in Figures 14 and 15.

It can be seen from Figure 14 that with the increase of the dynamic friction coefficient μ , the longitudinal maximum displacement of the main beam decreases, and with the increase of the R , the longitudinal maximum displacement of the main beam increases. Therefore, the longitudinal maximum displacement of the main beam depends on the coefficient of dynamic friction μ and the curvature radius R . When the $\mu < 0.06$, both μ and R have significant control effects on the displacement of the main beam. However, when the $\mu = 0.06$, the influence of R gradually weakened, and the sensitivity of the main beam displacement to the μ change decreased. When $\mu = 0.10$, the influence of μ and R on the displacement of the main beam becomes minimal, and further increasing R and μ cannot effectively reduce the displacement of the main beam.

As shown in Figure 15, the maximum bending moment of the pier top is first reduced, and then it becomes stable with the increase of R . When R remains constant, the bending moment of the pier top is firstly decreased and then increased with the increase of μ . When $\mu=0.04$, the bending moment at the top of the pier is the smallest, which shows that the damping effect of the friction pendulum isolation is the best. The change rule of pier top displacement is basically the same as that of the bending moment of pier top. When $\mu=0.04$, the displacement of the pier top is also the smallest, which reflects the best displacement control effect. Similarly, according to the existing reference [4], there exists a particular value of the friction coefficient of the friction pendulum isolation for which the structure response of the isolated bridge reaches the minimum value.

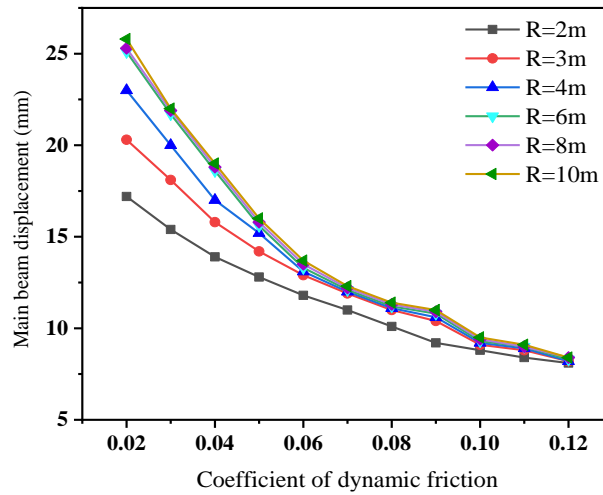


Figure 14. Relationship between the maximum displacement of the main beam and μ and R

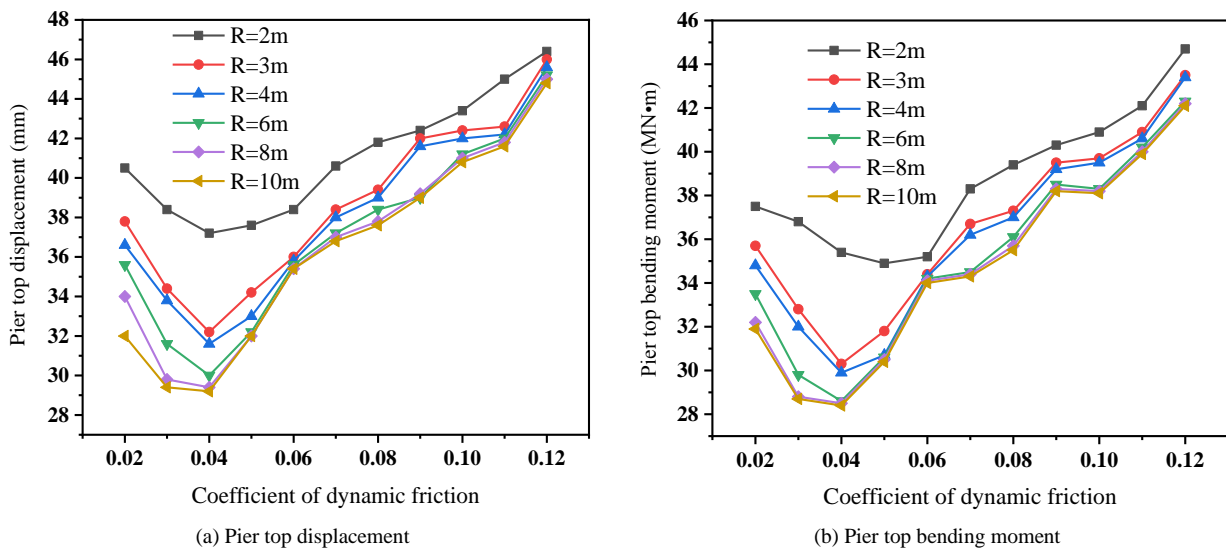


Figure 15. Relationship between the maximum bending moment and the maximum displacement of the pier with μ and R

When the dynamic friction coefficient of the friction pendulum isolation is constant, the maximum displacement and the maximum bending moment of the pier top decrease with the increase of the radius of curvature R , but the decreasing trend gradually weakens. Table 4 further compares the damping performance of friction pendulum isolation under different radius of curvature when the optimal dynamic friction coefficient is adopted.

Table 4. Pier top displacement and pier bending moment under different R ($\mu=0.04$)

Radius of curvature (m)	Pier top displacement (mm)	Change ratio	Pier top bending moment (MN·m)	Change ratio
2	37.2	—	35.3	—
3	32.2	13.4%	30.3	14.2%
4	31.6	1.9%	29.8	1.7%
6	30.0	5.1%	28.5	4.4%
8	29.4	2.0%	28.3	0.7%
10	29.2	0.7%	28.1	0.7%

As shown in Table 4, when R increases from 2m to 3m, the displacement of the pier top decreases from 37.2mm to 32.2mm, which is reduced by 13.4%, and the bending moment at the pier top is reduced from 35.3 MN·m to 30.3 MN·m, which is reduced by 14.2%. When R increases from 3m to 10m, the displacement of the pier top is only reduced by 9.3%, and the bending moment of the pier top is only reduced by 7.3%, which indicates that when the radius of curvature R exceeds 3m, the continuous increase of the radius of curvature has no significant influence on the damping property of the friction pendulum isolation, and it has no economic benefit.

To sum up, under the premise of ensuring the allowable displacement of the design of the friction pendulum isolation, in order to give full play to the shock absorption energy dissipation capacity of the friction pendulum isolation, the recommended friction coefficient is close to 0.04, and R should not be too large; on the whole, the comprehensive benefit is the best when R is taken as 3 m. Besides, the specific value should be determined according to the vertical bearing capacity and design displacement of the bridge.

8. Conclusions

On the background of practical engineering, the three-dimensional calculation model of long-span corrugated steel web bridges is established. The damping effect of friction pendulum isolation is studied by the response spectrum method and time history analysis method, and the influence of parameters is analyzed. The main conclusions are as follows:

- The vibration frequency of the bridge with friction pendulum isolation is always lower than that of the bridge with ordinary fixed bearings, and the relative difference reaches up to 35.0%.
- The friction pendulum isolation effectively separates the superstructure of the bridge from the substructure, thereby isolating most of the seismic wave energy and reducing the seismic responses.
- By comparing and analyzing the seismic responses of the bridge with ordinary fixed bearings and friction pendulum bearings, it is obtained that the friction pendulum isolation can not only effectively improve the stress state of the main beam and the bridge pier, but also reduce the displacement and acceleration of the pier top, so as to achieve the purpose of shock absorption, and the damping ratio is more than 50%.
- With the increase of the dynamic friction coefficient, the damping performance of the friction pendulum isolation shows a tendency to increase firstly and then decrease, and there is an optimal dynamic friction coefficient of 0.04. With the increase of the radius of curvature, the damping performance also shows a change of first increasing and then basically stable, and the optimum curvature radius is 3 m.
- Relying on the friction pendulum isolation alone is easy to lead to the increase of the displacement of the main beam, which may lead to other problems. In order to reduce the residual displacement and peak displacement of a friction pendulum isolation bridge, it is necessary to carry out the corresponding self-resetting and limiting research. For bridges using friction pendulum isolation, a variety of factors should be considered comprehensively in the design of seismic reduction and isolation so as to accurately evaluate the damping amplitude and achieve the best damping effect.

9. Declarations

9.1. Author Contributions

Conceptualization, Z.W. and W.J.; methodology, W.J. and J.H.; software, J.H.; validation, J.H.; formal analysis, J.H.; investigation, J.H.; resources, Z.W. and W.Z.; data curation, J.H. and W.Z.; writing—original draft preparation, J.H.; writing—review and editing, Z.W. and W.J.; visualization, J.H. and W.Z.; supervision, Z.W. and W.J.; project administration, Z.W. and W.J.; funding acquisition, Z.W. and W.J. All authors have read and agreed to the published version of the manuscript.

9.2. Data Availability Statement

The data presented in this study are available in the article.

9.3. Funding and Acknowledgements

This paper is a part of the Science and Technology Research Project of the Fourth Engineering Bureau of China Construction (Grant No. CSCEC4B-2023-KTA-17).

9.4. Conflicts of Interest

The authors declare no conflict of interest.

10. References

- [1] Zhan, Y. L., Zhang, L., Zhang, Q., & Jiang, Z. X. (2018). Effects of Parameters of Friction Pendulum Bearings on Seismic Responses of Seismically Isolated Bridge. *Bridge Construction*, 48(3), 45–49.
- [2] Zhang, J., Li, Y., & Zhang, C. (2024). Pounding induced overturning resistance of FPB-isolated structures considering soil-structure-interactions. *Soil Dynamics and Earthquake Engineering*, 177, 108416. doi:10.1016/j.soildyn.2023.108416.
- [3] He, W., Jiang, L., Wei, B., & Wang, Z. (2021). Influence of pier height on the effectiveness of seismic isolation of friction pendulum bearing for single-track railway bridges. *Smart Structures and Systems*, 28(2), 213–228. doi:10.12989/sss.2021.28.2.213.
- [4] Li, B., Wang, B., Wang, S., & Wu, X. (2020). Energy response analysis of continuous beam bridges with friction pendulum bearing by multihazard source excitations. *Shock and Vibration*, 2020, 1–17. doi:10.1155/2020/3724835.
- [5] Chen, X., Wu, P., & Li, C. (2022). Seismic performance assessment of base-isolated tall pier bridges using friction pendulum bearings achieving resilient design. *Structures*, 38, 618–629. doi:10.1016/j.istruc.2022.02.032.
- [6] Meng, D., Hu, S., Yang, M., Hu, R., & He, X. (2023). Experimental evaluation of the seismic isolation effectiveness of friction pendulum bearings in bridges considering transverse poundings. *Soil Dynamics and Earthquake Engineering*, 170, 107926. doi:10.1016/j.soildyn.2023.107926.
- [7] Gino, D., Miceli, E., & Castaldo, P. (2022). Seismic reliability analysis of isolated deck bridges using friction pendulum devices. *Procedia Structural Integrity*, 44, 1435–1442. doi:10.1016/j.prostr.2023.01.184.
- [8] Gupta, P. K., Agrawal, S., Ghosh, G., S, P., Kumar, V., & Paramasivam, P. (2023). Seismic behaviour of the curved bridge with friction pendulum system. *Journal of Asian Architecture and Building Engineering*, 1–14. doi:10.1080/13467581.2023.2292089.
- [9] Zhao, G., He, H., Ma, Y., & Yang, H. (2023). Analysis on seismic response of frictional pendulum isolated bridges limited by Rotational Mass Friction Damper. *China Civil Engineering Journal*, 56(2), 46–57. doi:10.15951/j.tmgxcb.2022.0403.
- [10] Li, C., Zhang, P., Li, Y., & Zhang, J. (2023). Effects of friction pendulum bearing wear on seismic performance of long-span continuous girder bridge. *Journal of Vibroengineering*, 25(3), 506–521. doi:10.21595/jve.2022.22915.
- [11] Wang, B., Xiao, Z., Zou, W., & Xu, Y. (2023). Experimental investigation on the broke force of shear pin for friction pendulum bearing. *Earthquake Engineering and Engineering Dynamics*, 43(5), 112–119. doi:10.13197/j.eeed.2023.0511.
- [12] Cao, S., Ozbulut, O. E., Dang, X., & Tan, P. (2024). Experimental and numerical investigations on adaptive stiffness double friction pendulum systems for seismic protection of bridges. *Soil Dynamics and Earthquake Engineering*, 176, 108302. doi:10.1016/j.soildyn.2023.108302.
- [13] Wei, B., Yang, Z., Xiao, B., Jiang, L., & Yu, Y. (2024). Simplified design theory of variable curvature friction pendulum bearing with adaptive capability and its application in railway bridge. *Structures*, 63, 106370. doi:10.1016/j.istruc.2024.106370.
- [14] Chang, H., Liu, L., Yang, S., & Liu, X. (2024). Seismic isolation effect of tunable friction pendulum system in bridge. *Australian Journal of Structural Engineering*, 25(2), 212–224. doi:10.1080/13287982.2023.2293319.
- [15] Liu, Q., J, N. S., & Xu, L. (n.d.). Seismic isolation analysis of corrugated steel web continuous girder bridge with long span and long segment. *Journal of China & Foreign Highway*, 39(3), 119–124.
- [16] Han, M., Dong, Y., Wang, T., Du, M., & Gao, Q. (2024). Fragility Assessment of a Long-Unit Prestressed Concrete Composite Continuous Girder Bridge with Corrugated Steel Webs Subjected to Near-Fault Pulse-like Ground Motions Considering Spatial Variability Effects. *Buildings*, 14(2), 330. doi:10.3390/buildings14020330.
- [17] Wei, B., Wan, K., Wang, W., Hu, Z., Jiang, L., & Li, S. (2023, May). Seismic isolation effect of a new type of friction pendulum bearing in high-speed railway girder bridge. *Structures*, 51, 776–790. doi:10.1016/j.istruc.2023.03.077.
- [18] Zhu, S. Y. (2013). The webs' stability analysis of long-span corrugated steel web PC box-girder bridges. Chongqing Jiaotong University, Chongqing, China. (In Chinese).
- [19] Guo, Y. (2021). Study on static and dynamic performance of single box three-cell PC box girder bridges with corrugated steel webs with variable cross-sections. Taiyuan University of Technology, Taiyuan, China. (In Chinese).
- [20] Xiao, L. (2020). Study on long period ground motion response and damping of flexible bridges based on response spectrum modification. Wuhan University of Technology, Wuhan, China. (In Chinese).
- [21] JTG/TB02-01-2008. (2008). Guidelines for seismic design of highway bridges. People's Communications Press, Beijing, China. (In Chinese).
- [22] Newmark, N. M. (1959). A Method of Computation for Structural Dynamics. *Journal of the Engineering Mechanics Division*, 85(3), 67–94. doi:10.1061/jmcea3.0000098.
- [23] Jia, Y., Zhao, R., Liao, P., Zhan, Y., & Li, F. (2018). Parameter Optimization and Damping Effect of Hyperbolic Surface Friction Pendulum Bearing for Continuous Girder Bridge under Rare Earthquake. *China Railway Science*, 39(3), 31–40. doi:10.3969/j.issn.1001-4632.2018.03.05.